AGU PUBLICATIONS

JGR

Journal of Geophysical Research: Planets

RESEARCH ARTICLE
10.1002/2016JE005122

Key Points:
- Hemispheric maps (2008–2015) are processed to explore Saturn's vortices.
- Spatio-temporal variations of Saturn's vortices are revealed.
- Physics behind the variability of Saturn's vortices needs more studies.

Correspondence to:
L. Li,
lli7@central.uh.eduu

Citation:
Trammell, H. J., et al. (2016), Vortices in Saturn's Northern Hemisphere (2008–2015) observed by Cassini ISS, *J. Geophys. Res. Planets*, *121*, 1814–1826, doi:10.1002/2016JE005122.

Received 28 JUN 2016
Accepted 2 SEP 2016
Accepted article online 8 SEP 2016
Published online 30 SEP 2016

Vortices in Saturn's Northern Hemisphere (2008–2015) observed by Cassini ISS

Harold Justin Trammell[1], Liming Li[2], Xun Jiang[1], Yefeng Pan[2], Mark A. Smith[3], Edgar A. Bering III[2], Sarah M. Hörst[4], Ashwin R. Vasavada[5], Andrew P. Ingersoll[6], Michael A. Janssen[5], Robert A. West[5], Carolyn C. Porco[7], Cheng Li[6], Amy A. Simon[8], and Kevin H. Baines[5]

[1]Department of Earth and Atmospheric Sciences, University of Houston, Houston, Texas, USA, [2]Department of Physics, University of Houston, Houston, Texas, USA, [3]Department of Chemistry, University of Houston, Houston, Texas, USA, [4]Department of Earth and Planetary Sciences, The Johns Hopkins University, Baltimore, Maryland, USA, [5]Jet Propulsion Laboratory, California Institute of Technology, Pasadena, California, USA, [6]Division of Geological and Planetary Sciences, Caltech, Pasadena, California, USA, [7]Space Science and Engineering Center, University of Wisconsin-Madison, Madison, Wisconsin, USA, [8]NASA Goddard Space Flight Center, Greenbelt, Maryland, USA

Abstract We use observations from the Imaging Science Subsystem on Cassini to create maps of Saturn's Northern Hemisphere (NH) from 2008 to 2015, a time period including a seasonal transition (i.e., spring equinox in 2009) and the 2010 giant storm. The processed maps are used to investigate vortices in the NH during the period of 2008–2015. All recorded vortices have diameters (east-west) smaller than 6000 km except for the largest vortex that developed from the 2010 giant storm. The largest vortex decreased its diameter from ~11,000 km in 2011 to ~5000 km in 2015, and its average diameter is ~6500 km during the period of 2011–2015. The largest vortex lasts at least 4 years, which is much longer than the lifetimes of most vortices (less than 1 year). The largest vortex drifts to north, which can be explained by the beta drift effect. The number of vortices displays varying behaviors in the meridional direction, in which the 2010 giant storm significantly affects the generation and development of vortices in the middle latitudes (25–45°N). In the higher latitudes (45–90°N), the number of vortices also displays strong temporal variations. The solar flux and the internal heat do not directly contribute to the vortex activities, leaving the temporal variations of vortices in the higher latitudes (45–90°N) unexplained.

1. Introduction

There are many compact vortices present in the atmosphere of Jupiter [e.g., *Smith et al*., 1979; *Ingersoll et al*., 1979; *Mitchell et al*., 1979; *Mac Low and Ingersoll*, 1986; *Morales-Juberias et al*., 2002; *Li et al*., 2004; *Trammell et al*., 2014]. In comparison, Saturn has fewer vortices in its atmosphere [*Vasavada et al*., 2006; *Trammell et al*., 2014]. These vortices play important roles in the atmospheric systems of the gas giant planets [e.g., *Ingersoll et al*., 2004; *Vasavada and Showman*, 2005; *Del Genio et al*., 2009]. Analyzing the vortex characteristics from observations along with chemical and physical models not only enriches our knowledge of vortices but also helps us better understand large-scale atmospheric dynamics [e.g., *Ingersoll and Cuong*, 1981; *Williams and Yamagata*, 1984; *Dowling and Ingersoll*, 1989; *Marcus et al*., 2000; *Li et al*., 2006; *Showman*, 2007; *del Rio-Gaztelurrutia et al*., 2010].

Observations by the Cassini spacecraft provide an opportunity to explore vortices on Saturn at unprecedented spatial resolution and over relatively long time scales. *Vasavada et al*. [2006] analyzed the Cassini observations and characterized Saturn's vortices in the Southern Hemisphere (SH). *Trammell et al*. [2014] conducted a global survey of Saturn's vortices. Based on the Cassini observations from 2008 to 2015, we process Saturn's maps and further study the temporal variations of vortices. The time period of 2008–2015 includes a seasonal transit (i.e., northern spring equinox in August 2009), so the processed maps provide a great opportunity to examine the seasonal variations of Saturn's vortices. In addition, a giant storm developed in 2010–2011 [*Sanchez-Lavega et al*., 2011; *Fischer et al*., 2011; *Fletcher et al*., 2011], and hence, we can explore the interaction between the giant storm and vortices. The processed maps from 2008 to 2015 resulting in this manuscript will be archived on the Planetary Data System to benefit other studies of Saturn's atmosphere.

2. Cassini Observations and Data Processing

The analyses of the temporal variations of Saturn's vortices are based on maps created from the images recorded by the Imaging Science Subsystem (ISS) on board Cassini [*Porco et al*., 2004]. We mainly use ISS

Table 1. Cassini/ISS Observational Parameters for the CB2 Images Used to Make the NH Maps From 2008 to 2015[a]

Time	Solar Longitude	Subsolar Latitude	Spatial Resolution
26 Feb 2008	341.5°	8.18°S	~94 km/pixel
25 Sep 2010	13.8°	6.12°N	~147 km/pixel
5 Mar 2011	19.1°	8.50°N	~191 km/pixel
8 Jan 2012	29.2°	12.65°N	~110 km/pixel
28 Feb 2013	42.5°	17.70°N	~56 km/pixel
14 Sep 2014	60.1°	22.95°N	~239 km/pixel
6 Sep 2015	71.0°	25.18°N	~76 km/pixel

[a]We could not find high-quality Cassini/ISS images to make the 2009 NH map with enough spatial coverage. Solar longitude is defined as the angular distance along Saturn's orbit around the Sun measured from northern spring equinox (0°). The solar longitude is used to differentiate different seasons on Saturn (i.e., northern spring 0–90°, northern summer 90–180°, northern autumn 180–270°, and northern winter 270–360°). Subsolar latitude is the latitude on a planet where the solar insolation is normal to the reference surface of Saturn (i.e., 1 bar pressure level).

images at the second continuum wavelength band filter (CB2~752 nm), which records more images than any other ISS filters. The ISS images at the strongest methane filter (MT3~890 nm), which probe higher altitude of Saturn's atmosphere than that of the CB2 images, are also utilized to explore the vertical structures of vortices. The data processing, which includes selecting, navigating, illumination-removing, projecting, and map-making, was introduced in our previous studies [*Vasavada et al*., 2006; *Trammell et al*., 2014]. The ring shadow was significant in the Northern Hemisphere (NH) before 2008, which makes it hard to make the NH maps with enough effective area. Making the maps of the Southern Hemisphere (SH) with good spatial coverage after 2010 is also hard due to the ring shadowing. In addition, the emphasis of the Cassini ISS observational mode was put on the polar region of the NH in recent years, which adds to the difficulty of making the SH maps after 2010. Therefore, we focus on the NH maps from 2008 to 2015 to investigate the temporal variations of Saturn's vortices. For the comparative studies of vortices between the NH and the SH, please refer to our previous study [*Trammell et al*., 2014].

The Cassini ISS data sets of making the NH maps are summarized in Table 1. We use the solar longitude to define the seasonal variation. The solar longitude varied from ~341.5° in 2008 (late NH winter) to ~71.0° in 2015 (late NH spring). The corresponding subsolar latitude moved from the SH (e.g., 8.18°S in 2008) to the NH (e.g., 25.18°N in 2015) during the time period of 2008–2015. Table 1 also shows that the spatial resolution of the selected Cassini ISS images roughly varies between ~100 km/pixel and ~200 km/pixel except for the selected images for the 2013 NH map (56 km/pixel). The ISS images with spatial resolutions coarser than 250 km/pixel fail to resolve the structure of vortices well and are not processed in this study. On the other hand, the images with very high spatial resolutions ($<$50 km/pixel) are not suitable for building global/hemispheric maps either. These images generally have spatial coverage less than 30° in the latitude or longitude direction, so it is difficult to combine them to cover the entire globe or hemisphere. Based on the spatial resolution in Table 1, we only record vortices with relatively large scales (i.e., east-west diameter larger than 1000 km) so that the structures are well resolved in the processed maps [*Trammell et al*., 2014]. Our tests suggest that varying spatial resolution (56–239 km/pixel) of our processed maps basically does not affect the recording of these relatively large vortices ($>$1000 km).

In most years, the NH maps are produced by approximately five to eight images with a spatial resolution of ~100–200 km/pixel and a time interval of ~1–2.5 h. Each of the five to eight images has spatial coverage ~50–70°W in the longitude direction and ~0–85°N in the latitude direction. For the 2013 map, only high-spatial resolution (56 km/pixel) images were available and 14 images are necessary to make the NH map, although observational gaps still exist. The uncertainty related to the observational gaps in recording vortices is discussed in the next section. For 2009, we could not find suitable groups of images to compose a NH map due to relatively sparse imaging during this time.

3. Results

Figures 1 and 2 display the processed NH maps during the period of 2008–2015. The processed NH maps are used to record all vortices with a length scale larger than 1000 km. In this study, the vortices are defined as the cloud features with the compact oval shapes because previous studies [*Li et al*., 2004; *Vasavada et al*., 2006;

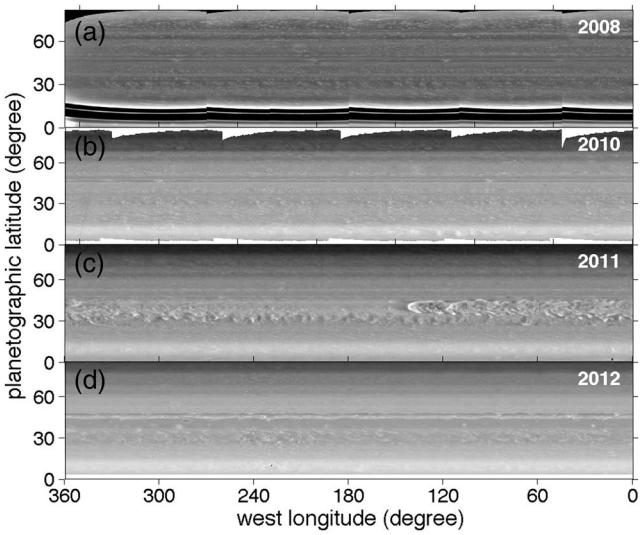

Figure 1. Processed NH maps in (a) 2008, (b) 2010, (c) 2011, and (d) 2012 based on the CB2 images recorded by the Cassini/ISS. The basic information of these CB2 images is presented in Table 1. The dark areas near the equator in 2008 (Figure 1a) are due to the ring shadow. The white areas in 2010 (Figure 1b) are observational gaps. As discussed in the text, a map was not produced for 2009 because the necessary data were not available from the Cassini ISS.

del Rio-Gaztelurrutia et al., 2010; *Sayanagi et al*., 2013] suggest that these cloud features have rotating motions. The basic characteristics of vortices (e.g., size, location, color/category, and vorticity) are analyzed with the processed NH maps.

Before investigating the vortices recorded by the NH maps, we first discuss Saturn's zonal winds (Figure 3), which are used to estimate the vorticity and meridional drifting of vortices. The zonal winds are based on a previous study [*García-Melendo et al*., 2011] with a new rotation rate of Saturn's magnetic field [*Read et al*., 2009] from the Cassini observations. The new reference system—system IIIw [*Read et al*., 2009]—suggests that Saturn's zonal winds flow to both east and west in the middle and high latitudes (Figure 3a). Figure 3 also shows the planetary vorticity (i.e., Coriolis parameter f), the relative vorticity of zonal winds ($-U_y = -\partial U/\partial y$), and their meridional gradients ($\beta = \partial f/\partial y$ and $-U_{yy} = -\partial^2 U/\partial y^2$). The gradient of total vorticity ($\beta - U_{yy}$) shown in Figure 3d is used to determine the meridional drifting of vortices by the mechanism of beta drift effect [*Holton*, 2004]. The vorticity gradient is also useful to discuss the barotropic stability and hence a possible generating mechanism of vortices.

Figures 4–10 show all vortices recorded from the NH maps in 2008, 2010, 2011, 2012, 2013, 2014, and 2015, respectively. The vortices in the NH are organized into the four categories defined by *Vasavada et al*. [2006]: (1) dark, (2) dark with a bright margin, (3) bright centered, and (4) bright. The vorticity of vortices is also estimated by following a method in the previous studies [*Vasavada et al*., 2006; *Trammell et al*., 2014], in which the vorticity of each vortex is estimated by the vorticity of the background zonal winds (Figure 3b). Table 2 summarizes the numbers of cyclonic/anticyclonic vortices and the vortices in the four categories during the period of 2008–2015. It suggests that the numbers of vortices in categories 2 (i.e., dark with a bright margin) and 4 (i.e., dark) are dominant among the four categories (55 out of the total 69 vortices). Examining the latitudinal location of vortices (Figures 4–10), we found that most of the vortices (18 out of 32) belong to category 2 in the polar region (i.e., >60°N). Table 2 also shows that there are more cyclonic vortices (50) than anticyclonic vortices (19) in the NH during the period of 2008–2015. Figures 6–10 suggest that all vortices generated in the latitude belt of the 2010 giant storm (25–45°N) are cyclonic except for the largest vortex and a small vortex at ~41–42°N in 2011 (Figure 6). On Jupiter, most vortices with

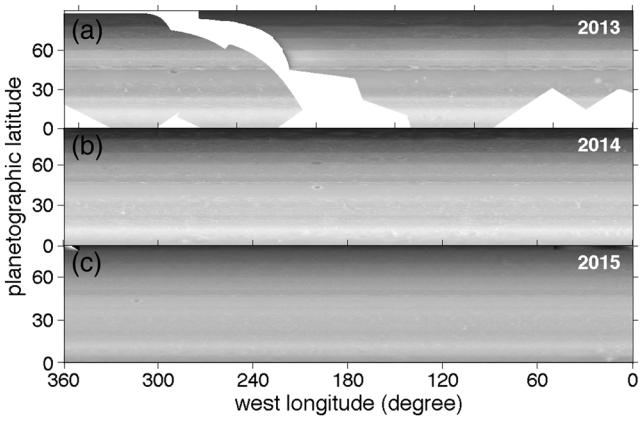

Figure 2. Same as in Figure 1 except for the NH maps in 2013, 2014, and 2015. The NH maps in 2014 and 2015 are built with five and six ISS raw images, respectively. The 2013 NH map was built with 14 images with relatively small spatial coverage, and the resulting map has large observational gaps.

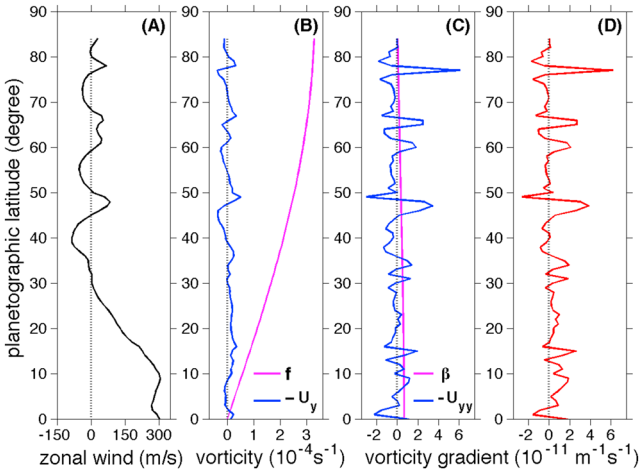

Figure 3. Saturn's zonal winds and vorticities. (a) Saturn's zonal winds. The zonal winds come from previous Cassini measurements [*García-Melendo et al.*, 2011], which are referenced with a new rotation period (i.e., system IIIw) [*Read et al.*, 2009] and further averaged over 1° latitude bins. (b) Planetary vorticity f and relative vorticity $-U_y$. (c) Medirional gradients of planetary vorticity and relative vorticity (β and $-U_{yy}$). (d) Meridional gradient of absolute vorticity ($\beta - U_{yy}$).

the compact oval shapes are anticyclonic [*Li et al.*, 2004]. The different behaviors in the vorticity of vortices between Jupiter and Saturn probably suggest different vortex dynamics between the two giant planets.

Based on Figures 4–10, we count the number of all vortices in the NH in each year of the period of 2008–2015. The number of vortices in each NH map is used to represent the average number of vortices in the corresponding year. Temporal variation of the number of vortices within a given year is possible, but determination of relatively short time scale variations is not possible due to the difficulty of making multiple NH maps in a given year (see section 2). Figure 11 suggests that the numbers of vortices experienced dramatic variation from 2008 to 2015. The numbers of recorded vortices from the NH maps represent the lower limits because the NH maps are not complete due to rings' effects and observational gaps (Figures 1 and 2). The error bars shown in Figure 11 are estimated by a method discussed in our previous study [*Trammell et al.*, 2014], in which the uncertainty in the total number of vortices is computed by the product of the number of observed vortices and the ratio of the area of the observational gaps to the observed area. Figure 11 shows that the number of vortices decreased from 12 ± 3 in 2008 to 7 ± 1 in 2010.

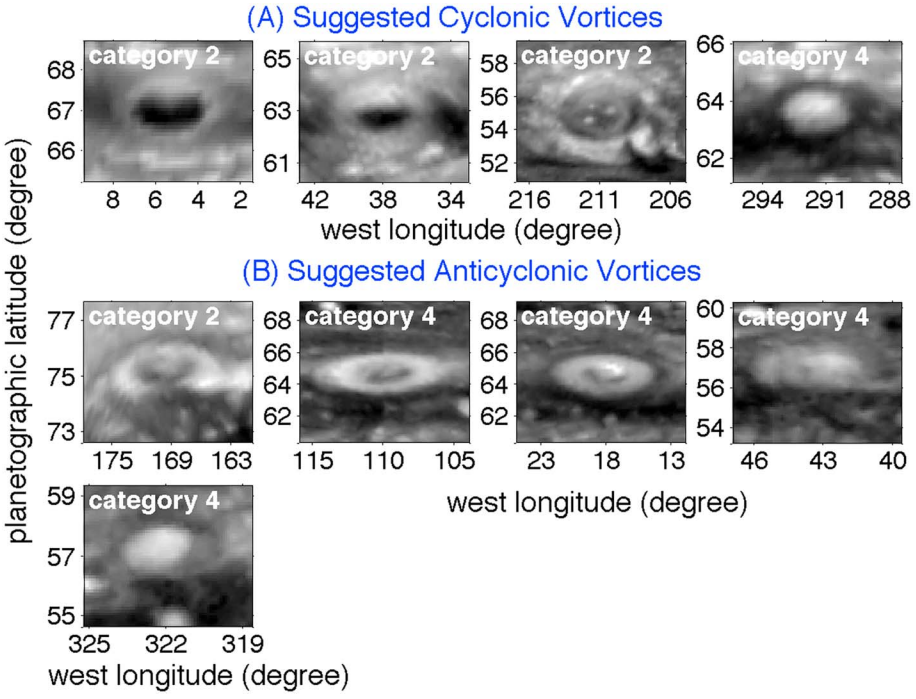

Figure 4. Vortices recorded with the 2008 NH map (Figure 1a). The vortices are divided into two groups: (a) cyclonic vortices and (b) anticyclonic vortices, based on the vorticity of zonal winds (Figure 3). In addition, the vortices are grouped into four categories: (1) dark, (2) dark with a bright margin, (3) bright centered, and (4) bright.

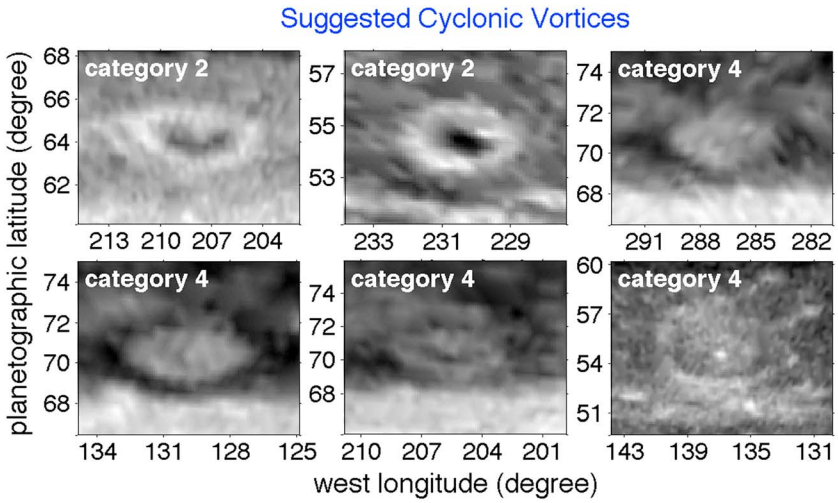

Figure 5. Same as in Figure 4 except for the vortices recorded with the 2010 NH map (Figure 1b).

Then the number continuously increased from 7 ± 1 in 2010 to 24 ± 5 in 2013. Finally, the number decreased from 24 ± 5 in 2013 to 6 ± 1 in 2015. The periodogram analysis of the numbers of vortices with the fast Fourier transform suggests there is a peak at a time period of ~5 years. However, the suggested 5 year periodic oscillation should be examined further with longer observations because the time period of current data (2008–2015) is too short.

Figure 12 suggests that most vortices are concentrated around the peaks of westward jets, as revealed in previous studies [*Vasavada et al*., 2006; *Trammell et al*., 2014]. The only exceptions are the vortices in the latitude band around 30°N, which is a region away from the westward jets. The vortices around 30°N and other vortices around 40°N developed in 2011–2015, following the giant storm in 2010. The NH map in 2011 (Figure 1c) further shows that these vortices are located inside the latitude belt of bright clouds generated from the giant storm (25–45°N). The maps from 2008 and 2010 (Figures 1a and 1b), prior to the eruption of the giant storm in the end of 2010, do not display any vortices in the latitude belt of the 2010 giant storm. Therefore,

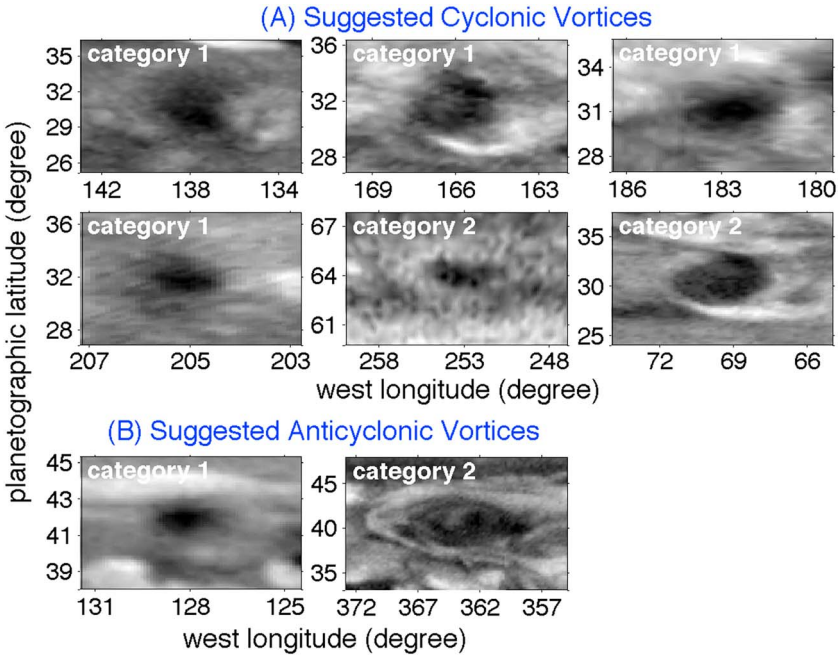

Figure 6. Same as in Figure 4 except for the vortices recorded with the 2011 NH map (Figure 1c).

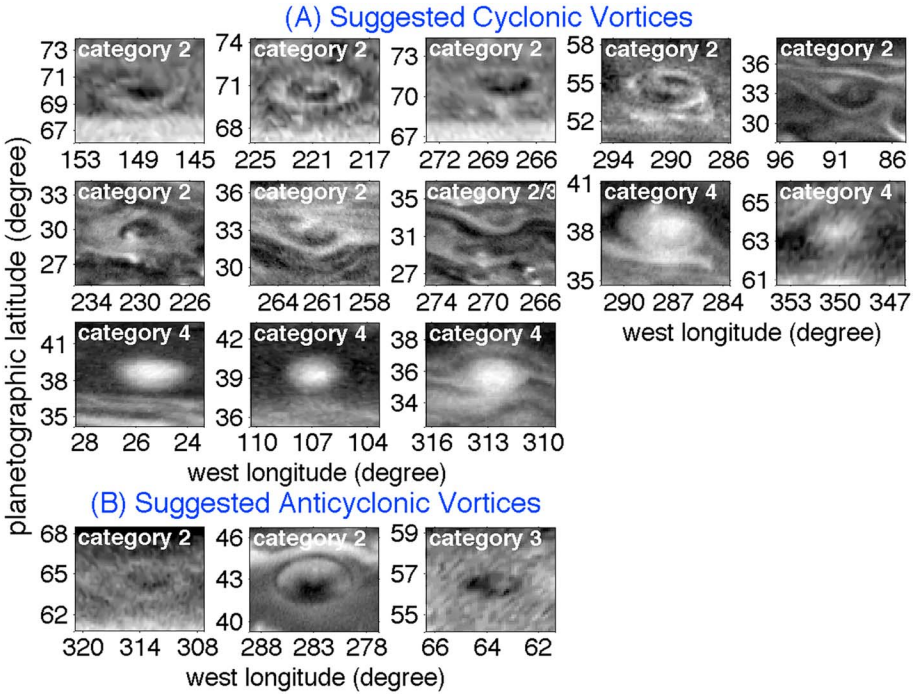

Figure 7. Same as in Figure 4 except for the vortices recorded with the 2012 NH map (Figure 1d). Note that there are two vortices in the third map of the second row, which belong to categories 2 and 3, respectively.

the midlatitude vortices are probably related to the activities of the 2010 giant storm. The 2010 giant storm died in the second half of 2011 [*Sayanagi et al.*, 2013]. The number of vortices in the latitude belt of the 2010 giant storm (25–45°N) began to decrease from 10 in 2012 to 2 in 2015, which also suggests that these vortices are related to the activities of the giant storm.

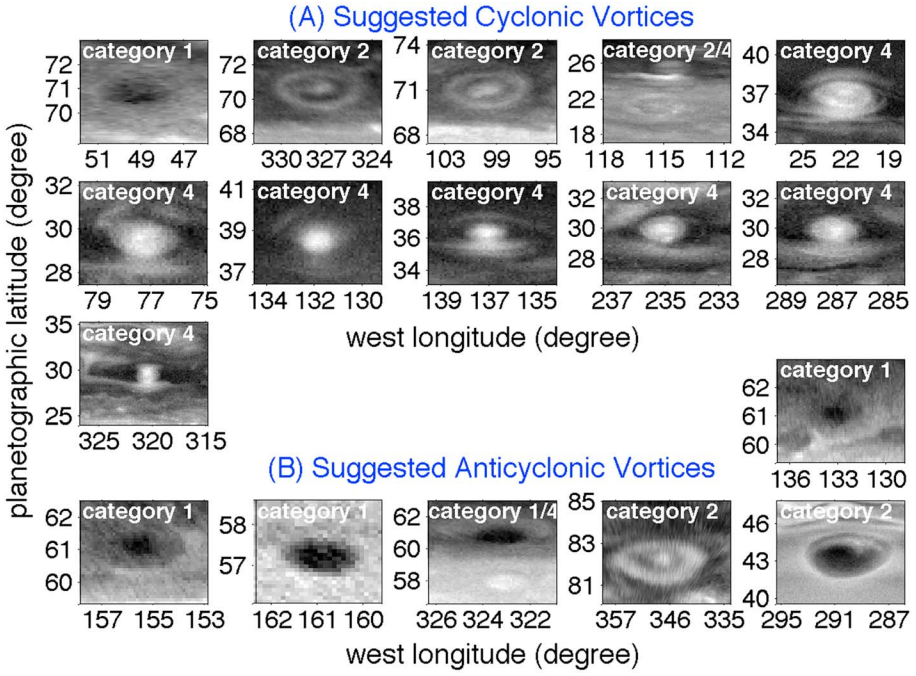

Figure 8. Same as in Figure 4 except for the vortices recorded with the 2013 NH map (Figure 2a). Note that there are two vortices in the fourth map of the first row, which belong to categories 2 and 4, respectively. There are also two vortices in the third map of the last row, which belong to categories 1 and 4, respectively.

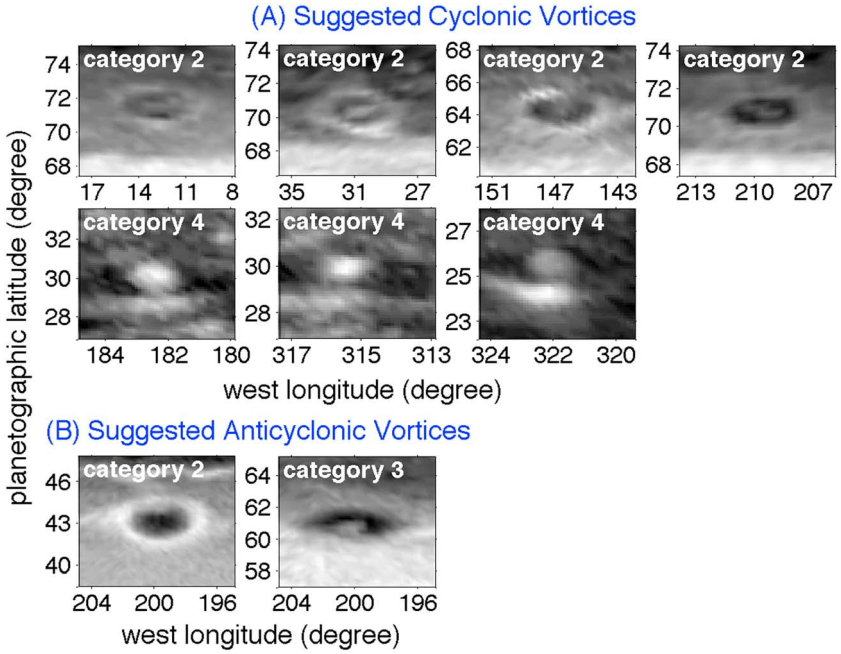

Figure 9. Same as in Figure 4 except for the vortices recorded with the 2014 NH map (Figure 2b).

Examining the latitude locations and structures of vortices in the latitude belt of the 2010 giant storm suggests that no vortices from the storm except for large vortices at ~40–43°N appear in consecutive NH maps, which suggests that most vortices generated in the storm belt have lifetimes shorter than 1 year. The large vortices around 40–43°N shown in Figures 6–10 are the same vortex even though their appearances and locations are different. Figure 13 shows the time series of the largest vortex from the 2010 giant storm. It suggests that the vortex decreased its size significantly from 10,658 km (east-west diameter) at the beginning of 2011 to 6528 km at the beginning of 2012, which is consistent with the shrinking of the vortex revealed in previous studies [*Fletcher et al*., 2012; *Sayanagi et al*., 2013]. Figure 13 further suggests that the size of the vortex continuously decreased from 2012 to 2014 (i.e., 6528 km in 2012, 5143 km in 2013, and 4658 km in 2014) and basically kept constant from 2014 to 2015 (i.e., 4658 km in 2014 and 4643 km in 2015). The time-average east-west diameter of the largest vortex is ~6500 km during the period of 2011–2015. The center of the vortex significantly changed from ~41°N in 2011 to ~43°N in 2012 and then basically kept constant at ~43°N afterward (2012–2015). The meridional movement of the largest vortex can be explained by the beta drift effect [*Holton*, 2004; *Sayanagi et al*., 2013]. Figure 3d shows that the gradient of the total vorticity ($\beta - U_{yy}$) in the latitude band of 41–43°N is negative, which suggests that vortices in this latitude band (41–43°N) should have poleward drifting if they are anticyclones [*Holton*, 2004]. This is consistent with the poleward drifting from ~41°N in 2011 to ~43°N in 2012 for the largest vortex with an anticyclone structure [*Sayanagi et al*., 2013]. Figure 3d further suggests that the gradient of the total vorticity is zero at ~43°N, which explains why the largest vortex stopped the poleward drifting around this latitude (43°N) since 2012.

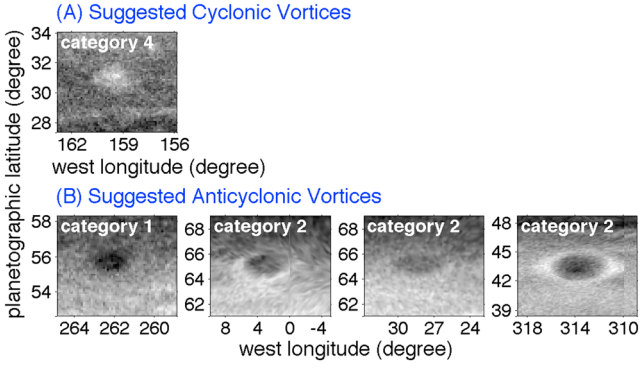

Figure 10. Same as in Figure 4 except for the vortices recorded with the 2015 NH map (Figure 2c).

In the equatorial region (0–25°N) outside the latitude belt of the giant storm (Figure 12), only one small vortex was present during the period

Table 2. Category and Vorticity of the Vortices in the NH During the Period of 2008–2015[a]

Suggested Cyclonic Vortices 50				Suggested Anticyclonic Vortices 19			
Category 1	Category 2	Category 3	Category 4	Category 1	Category 2	Category 3	Category 4
5	22	1	22	6	6	2	5

[a]The four categories of Saturn's vortices are defined by *Vasavada et al.* [2006]: (1) dark, (2) dark with a bright margin, (3) bright centered, and (4) bright. It should be mentioned that some vortices cannot be clearly grouped into the four categories, which are grouped into the closest categories. The vorticities of vortices are estimated by the vorticity of zonal winds. Most vortices counted in this table are different except for the large anticyclonic vortex at ~40–42°N, which came from the 2010 giant storm. The largest vortex is repeatedly counted in 2011, 2012, 2013, 2014, and 2015. Therefore, there is a total of 19 (23 − 4 = 19) anticyclonic vortices recorded in the NH during the period of 2008–2015.

of 2008–2015, occurring around 21°N in 2013, while Jupiter has no vortices in the equatorial region [e.g., *Li et al.*, 2004]. The strong eastward jets dominate the equatorial regions on Jupiter and Saturn. Previous studies suggest that atmospheric instability related to the westward jets contributes to the generation of vortices on the giant planets [*Dowling and Ingersoll*, 1989; *Li et al.*, 2004; *Vasavada et al.*, 2006; *Trammell et al.*, 2014]. One possible reason that the equatorial regions on Jupiter and Saturn lack vortices is that the eastward jets in the equatorial regions do not have such an instability mechanism to generate vortices. The Coriolis force, which helps the rotation of air parcels to facilitate the vortex development, is smaller in the low latitudes than in the middle and high latitudes. The small Coriolis force is one more factor for lacking vortices in the equatorial regions on Jupiter and Saturn. It should be mentioned that it is also possible that opacity from high-altitude hazes [e.g., *West*, 1983; *Perez-Hoyos and Sanchez-Lavega*, 2006a] makes it hard to detect equatorial vortices in the levels of visible clouds probed by the CB2 images.

In the high latitudes (45–90°N) outside the latitude belt of the giant storm (Figure 12), the number of vortices also displays strong temporal variations (nine in 2008, six in 2010, one in 2011, seven in 2012, nine in 2013, five in 2014, and three in 2015). Examination of the sizes, shapes, and locations of these vortices (Figures 3–9) suggests that most of them do not appear in consecutive maps, implying that these vortices have lifetimes shorter than 1 year. The only exception was a vortex near 65°N, which has a dark center and a bright margin with a size ~3000 km. This vortex seems to appear in all maps except for 2013. There are observational gaps in the polar region of 2013 map (Figure 2a), and it is possible that there is a similar vortex near 65°N in 2013. If so, there was always a vortex around 65°N from 2008 to 2015. The vortices around 65°N display small differences in appearance from year to year, which could reflect different evolutionary phases during the period of 2008–2015 if these vortices are in fact the same vortex. However, we cannot rule out the possibility that these vortices around 65°N in different years are different structures because we do not have continuous observations resolving their complete lifetimes.

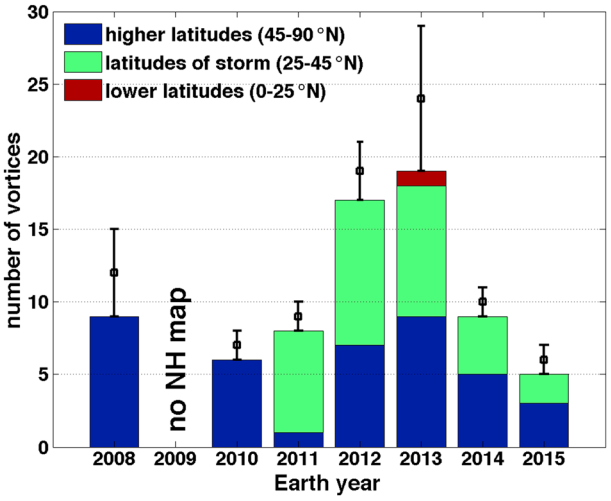

Figure 11. Numbers of the NH vortices (>1000 km) during the period of 2008–2015. Maps of the recorded vortices are shown in Figures 4–10. The numbers of recorded vortices represent the lower limits of the numbers, and the error bars are estimated based on observational gaps as discussed in the text.

The vortices in the polar region observed by Cassini during the period of 2008–2015 are different from the long-lived north polar vortex during the period of 1980–1995 reported by the Voyager spacecraft [*Smith et al.*, 1982], the Hubble Space Telescope [*Caldwell et al.*, 1993], and the Pic-du-Midi Observatory [*Sanchez-Lavega et al.*, 1993, 1997] for the long-lived polar vortex had a much larger size (7000–11,000 km) and a much longer lifetime (>15 years). The polar vortices recorded by Cassini (2008–2015) have much smaller sizes (~1500–3000 km). These polar vortices are mainly concentrated around the peaks of westward jets (Figure 12), where the atmosphere is barotropically unstable (Figure 3).

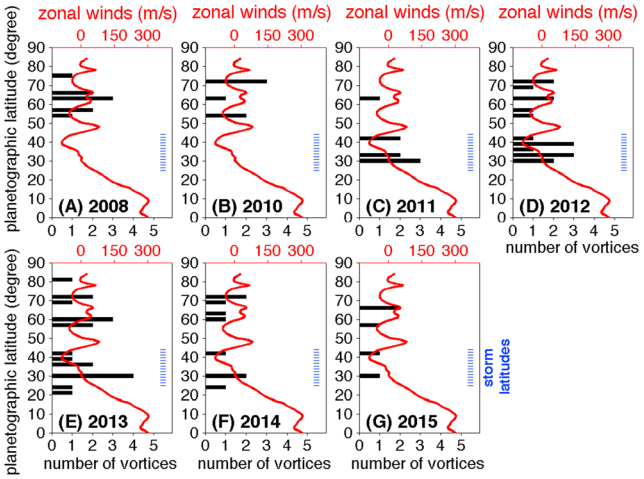

Figure 12. (a–g) Comparison between meridional distribution of vortices and zonal winds. The vortices are organized into 3° latitude bins. Saturn's zonal winds come from a combination of previous wind measurements [*García-Melendo et al.*, 2011] and a new rotation period [*Read et al.*, 2009] from the Cassini observations. The vertical dashed blue line in each plot represents the latitude range of bright clouds from the 2010 giant storm (25–45°N).

Therefore, the generating mechanism of these polar vortices is probably related to barotropic instability.

Even though most vortices observed by Cassini in the polar region and in the low/middle latitudes have short lifetimes, their appearances in both the continuum-filter images (CB2) and the strongest methane filter images (MT3) suggest that some of them have large vertical extents. We search for the simultaneous MT3 images for the vortices recorded in the CB2 images. Figure 14 shows the examples of the vortices appearing in both CB2 images MT3 images. The two filters (CB2 and MT3) have different sensing levels (CB2 at ~360 mbar and MT3 at ~60 mbar) [*Perez-Hoyos and Sanchez-Lavega*, 2006a; *Garcia-Melendo et al.*, 2010], which suggests that the vertical structures of these vortices showing in both CB2 and MT3 images are larger than vertical extension between 360 mbar and 60 mbar. The vertical extension between 360 mbar and 60 mbar is about 1.8 scale heights (~108 km with Saturn's scale height ~60 km). Figure 14 also reveals the different appearances of vortices between the CB2 and MT3 images, which implies that these vortices have different dynamical structures and chemical components at different pressure levels.

Figure 15 is a scatterplot of the sizes of vortices, which shows the aspect ratio (i.e., ratio between east-west diameter and north-south diameter). It suggests that all vortices except for the largest vortex from the 2010 giant storm have sizes smaller than 6000 km. This figure also suggests that about two thirds of vortices have east-west diameters larger than their north-south diameters. The remaining one third of vortices, which are generally small (i.e., $<$4000 km), have east-west diameters smaller than their north-south diameters. The linear fitting by the least squares method [*Bevington and Robinson*, 2003] suggests that the average ratios between east-west diameters and north-south diameters are 1.7 ± 0.3 and 2.0 ± 0.4 for cyclonic and anticyclonic vortices, respectively. The uncertainty of linear fitting is estimated by a method we previously developed [*Li et al.*, 2011a]. The average ratio of vortices does not significantly change between the cyclonic vortices and the anticyclonic vortices, which suggests that the average ratio of vortices mainly depends on the sizes of vortices instead of their vorticities.

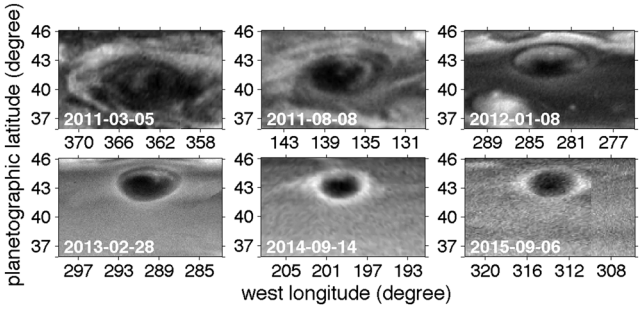

Figure 13. Time series of the largest vortex from the 2010 giant storm. Except for the second map, all maps of the largest vortex come from the processed NH maps (Figures 1 and 2). To better track the largest vortex, we search the ISS database and add one more map of the vortex on 8 August 2011 (second map of Figure 13), which is between the time of the first map (5 March 2011) and the time of the third map (8 January 2012).

The distribution of the sizes of vortices in the latitude direction is shown in Figure 16, which is further compared to the Rossby deformation radius. The Rossby deformation radius is given by $R = \sqrt{gH}/f$ [*Holton*, 2004; *Pedlosky*, 2008] for barotropic atmosphere, where g is the gravity, H is the height of the atmospheric layer we are studying, and f is the Coriolis parameter. Assuming that the atmospheric layer in which Saturn's vortices develop has a thickness comparable to the vertical extension between the pressure levels sensed by

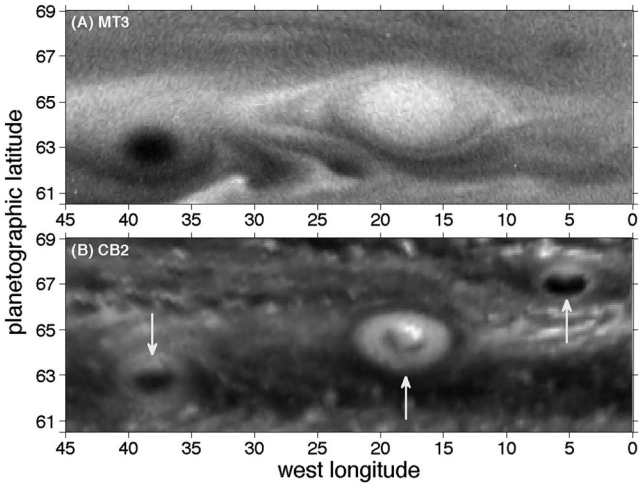

Figure 14. Examples of Saturn's vortices recorded by both of the two ISS filters (MT3 and CB2). (a) MT3 map and (b) CB2 map. The two maps have the same latitude and longitude ranges to facilitate the comparison. In addition, the CB2 and MT3 images, which are used to process the corresponding maps, were taken at intervals of 1 min and 20 s. So the two maps are nearly simultaneous. There are three white arrows pointing to the three vortices shown in the CB2 map. The CB2 map comes from the 2008 NH map shown in Figure 1a, and the three vortices are also shown in Figure 4.

the CB2 and MT3 filters (~108 km as discussed above), we have the Rossby deformation radius as a function of latitude (Figure 16). Figure 16 suggests that the maximal sizes of vortices within different latitude bins basically decrease from the equatorial region to the polar region except for the largest vortex from the 2010 giant storm (~42°N) and a few vortices in the equatorial region (~21–26°N) and the polar region (~82°N). Such a decrease trend is qualitatively consistent with the decreasing Rossby deformation radius in the latitude direction, which suggests that the mutual geostrophic adjustment between the mass field and the velocity field plays roles in the development of Saturn's vortices.

4. Conclusions and Discussions

The Cassini ISS images are processed into the NH maps to examine vortex activity on Saturn. The sizes of the recorded vortices in the NH are related to the Rossby deformation radius, which implies that the mutual geostrophic adjustment is important for the development of vortices. Two thirds of the vortices have larger sizes in the east-west direction than in the north-south direction. Our survey also suggests that the vortices in categories 2 (dark with a bright margin) and 4 (bright) are dominant in the NH (Table 2). The estimates of the vorticities of vortices from the zonal winds suggest that there are more cyclonic vortices than anticyclonic vortices in the NH, which is different from the dominant anticyclonic vortices on Jupiter.

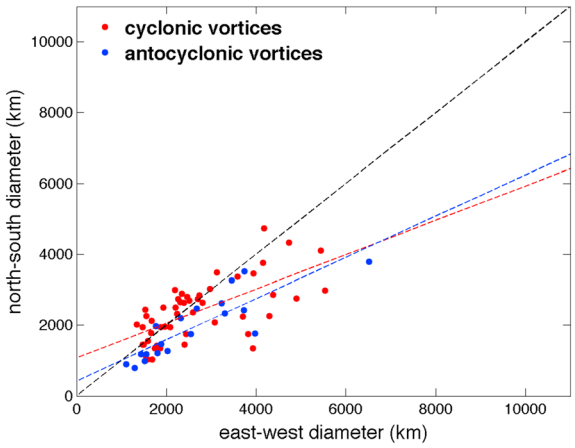

Figure 15. Scatterplot of vortices. Vortices are divided into two groups (cyclonic versus anticyclonic). For the largest vortex from the 2010 giant storm, which is anticyclonic, we average its size during the period of 2011–2015. The lines with red and blue colors are the fitting lines for the ratios of the east-west diameters to the north-south diameters for the cyclonic and anticyclonic vortices, respectively. The dashed black line represents the ratio as 1.0 (i.e., the east-west diameters are equal to the north-south diameters).

The number of vortices in the NH displays significantly temporal variations. The spatial distribution of vortices suggests different behaviors in different latitude regimes. In the middle latitudes in which the 2010 giant storm developed (i.e., 25–45°N), vortex activity is primarily affected by the giant storm. There is no vortex in the middle latitudes before the eruption of the giant storm (December 2010). Then the vortices became active with the development of the giant storm. In the equatorial region (0–25°N) outside the latitude belt of the giant storm, there is no vortex discovered during the period of 2008–2015 except for a small vortex in 2013. The equatorial region has strong eastward jets, which are barotropically stable. The lack of vortices in the equatorial region may be due to the lack of atmospheric

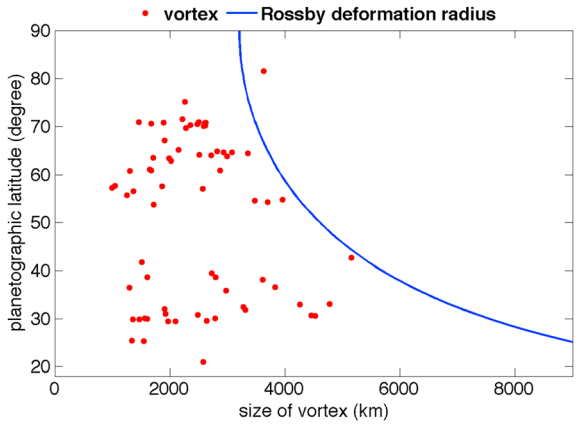

Figure 16. Sizes of vortices and Rossby deformation radius. The size of each vortex is defined as an average of the east-west diameter and the north-south diameter. The size of the largest vortex from the 2010 giant storm is averaged over the period of 2011–2015.

instability, since instability is a generating mechanism for vortices. The small Coriolis force in the equatorial regions also contributes to the lack of vortices in the equatorial region. In the high latitudes (45–90°N) outside the latitude belt of the giant storm, there is strong temporal variation of vortices during the period of 2008–2015.

The significant temporal variations in the behaviors (e.g., number, aspect ratio, category, and vorticity) of vortices in the NH are interesting. One possible cause of temporal variations is the seasonal change in solar flux. Figure 17 shows the solar flux at the top of Saturn's atmosphere, in which the Sun-Saturn distance and the effects of rings (e.g., scattering, shading, and emitting) are considered [*Hanel et al.*, 1983; *Barnet*, 1990; *Perez-Hoyos and Sanchez-Lavega*, 2006b; *Sanchez-Lavega et al.*, 2012; *Li et al.*, 2015]. The solar flux continuously increased from 2008 to 2015, so the seasonal variation of solar flux cannot explain the temporal oscillation in the number of vortices in any latitude region in the NH.

The internal heat can be the other possible candidate for the driving force of vortices and their temporal variation on Saturn. Saturn has a significant internal heat [*Hanel et al.*, 1983]. If Saturn's internal heat is concentrated in the latitude bands of vortices, its related vertical motions will help the development of some vortices on Saturn. However, the spatial distribution of internal heat on Saturn has not been determined yet [*Li et al.*, 2010]. The internal heat on the giant planets probably has time scales much longer than the orbital periods [*Flasar*, 1973]. Therefore, it seems that the internal heat is hard to explore the temporal variations of vortices at a relatively short time scale.

Regarding the effects of temporal variations of vortices on planetary atmospheres, one previous study of Jupiter [*Marcus*, 2004] suggested that the change in the total number of vortices is related to large-scale temperature variation. Studies of Saturn [e.g., *Achterberg et al.*, 2014; *Fletcher et al.*, 2016] indicated that atmospheric temperature at the pressure levels of visible clouds and vortices (~360 mbar) generally increased during the period of 2008–2015, while the strongest increase happened from 2010 to 2011 in the latitudes of the 2010 giant storm. The general increase in atmospheric temperature is different from the temporal oscillation in the number of vortices, which suggests that there is no direct relationship between large-scale variations of atmospheric temperature and the temporal variations of vortices. In addition, the larger-scale zonal winds at the pressure levels of visible clouds, in which the vortices are examined, did not show any significant temporal variations in most of the latitudes during the past few years [*García-Melendo et al.*, 2011; *Li et al.*, 2011b; *Blalock et al.*, 2014]. Therefore,

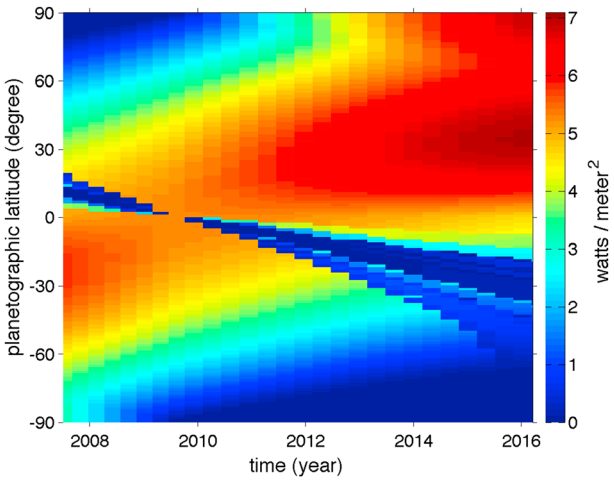

Figure 17. Incident solar flux at the top of Saturn's atmosphere from 2008 to 2016. Saturn's oblateness, orbital eccentricity, and rings' effects (blocking, scattering, and emitting) are considered based on the previous studies [*Hanel et al.*, 1983; *Barnet*, 1990; *Perez-Hoyos and Sanchez-Lavega*, 2006b; *Sanchez-Lavega et al.*, 2012; *Li et al.*, 2015].

the temporal variations of vortices do not directly affect the large-scale thermal structure and general circulation on Saturn.

It will be also interesting to examine the local temperature anomaly corresponding to the vortex development. Unfortunately, the spatial resolution of most retrieved temperature maps from the observations of the Cassini Composite Infrared Spectrometer (CIRS) cannot resolve vortices [e.g., *Li et al*., 2008] except for the largest one from the 2010 giant storm [*Fletcher et al*., 2011, 2016; *Achterberg et al*., 2014]. More importantly, a proposed Cassini project named "feature track," in which the Cassini ISS and CIRS simultaneously observe some interesting regions of Saturn, has not been fully conducted yet. Therefore, the simultaneous observations of Saturn's vortices from the Cassini ISS and CIRS are very limited. Further Cassini observations and theoretical studies are needed to fully understand the role of vortices in Saturn's atmosphere.

Acknowledgments
We gratefully acknowledge the Cassini ISS team for recording the raw data sets. We also acknowledge the support from the NASA ROSES Cassini Data Analysis and Participating Scientists program and Planetary Data Archiving, Restoration, and Tools program. Finally, we thank the two anonymous reviewers for providing their constructive suggestions to significantly improve the manuscript. We used the new Cassini data in 2015, which are not archived in the public Planetary Data System (PDS) (https://pds.nasa.gov) yet. The 2015 Cassini ISS raw data will be released by the Cassini ISS team and archived in the PDS in late 2016. We cannot archive the processed 2015 data before the release of the ISS raw data, so we plan to archive the data of the processed NH maps in the atmospheres node of PDS (http://atmos.pds.nasa.gov) in the beginning of 2017 or so.

References

Achterberg, R. K., P. J. Gierasch, B. J. Conrath, L. N. Fletcher, B. E. Hesman, G. L. Bjoraker, and F. M. Flasar (2014), Changes to Saturn's zonal-mean tropospheric thermal structure after the 2010-2011 northern hemisphere storm, *Astrophys. J.*, *786*, 92, doi:10.1088/0004-637X/786/2/92.

Barnet, C. D. (1990), Saturn's seasonal winds and temperature: The effect of the ring system on the troposphere and stratosphere, Thesis, New Mexico State Univ.

Bevington, P. R., and D. K. Robinson (2003), *Data Reduction and Error Analysis for the Physical Sciences*, 3rd ed., McGraw-Hill, New York.

Blalock, J. J., K. M. Sayanagi, A. P. Ingersoll, S. P. Shawn, and U. A. Dyudina (2014), Saturn's zonal winds at cloud level between 2004–2013 from Cassini ISS images. DPS meeting, *Bull. Am. Astron. Soc.*, *46*.

Caldwell, J., X.-M. Hua, B. Turgeon, J. A. Westphal, and C. D. Barnet (1993), An observed drift of Saturn's polar spot by HST, *Science*, *260*, 326–329.

Del Genio, A. D., R. K. Achterberg, K. H. Baines, F. M. Flasar, P. L. Read, A. Sánchez-Lavega, and A. P. Showman (2009), Saturn atmospheric structure and dynamics, in *Saturn From Cassini-Huygens*, edited by M. K. Dougherty, L. W. Esposito, and S. M. Krimigis, pp. 113-159, Springer, New York.

del Rio-Gaztelurrutia, T., J. Legarreta, R. Hueso, S. Perez-Hoyos, and A. Sanchez-Lavega (2010), A long-lived cyclone in Saturn's atmosphere: Observations and models, *Icarus*, *209*(2), 665–681.

Dowling, T. E., and A. P. Ingersoll (1989), Jupiter's Great Red Spot as a shallow water system, *J. Atmos. Sci.*, *46*, 3256–3278.

Fischer, G., et al. (2011), A giant thunderstorm on Saturn, *Nature*, *475*, 75–77.

Flasar, F. M. (1973), Gravitational energy sources in Jupiter, *Astrophys. J.*, *186*, 1097–1106.

Fletcher, L. N., et al. (2011), Thermal structure and dynamics of Saturn's northern springtime disturbance, *Science*, *332*, 1413–1417.

Fletcher, L. N., et al. (2012), The origin and evolution of Saturn's 2011-2012 stratospheric vortex, *Icarus*, *221*, 560–586.

Fletcher, L. N., P. G. J. Irwin, R. K. Achterberg, G. S. Orton, and F. M. Flasar (2016), Seasonal variability of Saturn's tropospheric temperatures, winds, and para-H_2 from Cassini far-IR spectroscopy, *Icarus*, *264*, 137–159.

Garcia-Melendo, E., A. Sanchez-Lavega, J. Legarreta, S. Perez-Hoyos, and R. A. Hueso (2010), A strong high altitude narrow jet detected at Saturn's equator, *Geophys. Res. Lett.*, *37*, L22204, doi:10.1029/2010GL045434.

García-Melendo, E., S. Pérez-Hoyos, A. Sánchez-Lavega, and R. Hueso (2011), Saturn's zonal wind profile in 2004–2009 from Cassini ISS images and its long-term variability, *Icarus*, *215*, 62–74.

Hanel, R. A., B. J. Conrath, V. G. Kunde, J. C. Pearl, and J. A. Pirraglia (1983), Albedo, internal heat-flux, and energy-balance of Saturn, *Icarus*, *53*, 262–285.

Holton, J. R. (2004), *An Introduction to Dynamic Meteorology*, 4th ed., Academic, San Diego, Calif.

Ingersoll, A. P., and P.-G. Cuong (1981), Numerical model of long-lived Jovian vortices, *J. Atmos. Sci.*, *38*, 2067–2074.

Ingersoll, A. P., R. F. Beebe, S. A. Collins, G. E. Hunt, J. L. Mitchell, P. Muller, B. A. Smith, and R. J. Terrile (1979), Zonal velocity and texture in the Jovian atmosphere inferred from Voyager images, *Nature*, *280*, 773–775.

Ingersoll, A. P., T. E. Dowling, P. J. Gierasch, G. S. Orton, P. L. Read, A. Sanchez-Lavega, A. P. Showman, A. A. Simon-Miller, and A. R. Vasavada (2004), Dynamics of Jupiter's atmosphere, in *Jupiter: The Planet, Satellites, and Magnetosphere*, edited by F. Bagenal, T. E. Dowling, and W. B. McKinnon, pp. 105–128, Cambridge Univ. Press, Cambridge.

Li, L., A. P. Ingersoll, A. R. Vasavada, C. C. Porco, A. D. Del Genio, and S. P. Ewald (2004), Life cycles of spots on Jupiter from Cassini images, *Icarus*, *172*, 9–23.

Li, L., A. P. Ingersoll, and X. L. Huang (2006), Interaction of moist convection with zonal jets on Jupiter and Saturn, *Icarus*, *180*, 113–123.

Li, L., P. J. Gierasch, R. K. Achterberg, B. J. Conrath, F. M. Flasar, A. R. Vasavada, A. P. Ingersoll, D. Banfield, A. A. Simon-Miller, and L. N. Fletcher (2008), Strong jet and a new thermal wave in Saturn's equatorial stratosphere, *Geophys. Res. Lett.*, *35*, L23208, doi:10.1029/2008GL035515.

Li, L., et al. (2010), Emitted power of Saturn, *J. Geophys. Res.*, *115*, E11002, doi:10.1029/2010JE003631.

Li, L., X. Jiang, M. T. Chahine, E. T. Olsen, E. Fetzer, L. Chen, and Y. L. Yung (2011a), Recycling rate of atmospheric moisture over the past two decades, *Environ. Res. Lett.*, *6*, doi:10.1088/1748-9326/6/3/034017.

Li, L., et al. (2011b), Equatorial winds on Saturn and the stratospheric oscillation, *Nat. Geosci.*, *4*, 750–752, doi:10.1038/NGEO1292.

Li, L., et al. (2015), Saturn's giant storm and global radiant energy, *Geophys. Res. Lett.*, *42*, 2144–2148, doi:10.1002/2015GL063763.

Mac Low, M. M., and A. P. Ingersoll (1986), Merging of vortices in the atmosphere of Jupiter: An analysis of Voyager images, *Icarus*, *65*, 353–369.

Marcus, P. S. (2004), Prediction of a global climate change on Jupiter, *Nature*, *428*, 828–831.

Marcus, P. S., T. Kundu, and C. Lee (2000), Vortex dynamics and zonal flows, *Phys. Plasmas*, *7*, 1630–1640.

Mitchell, J. L., R. J. Terrile, B. A. Smith, J.-P. Muller, A. P. Ingersoll, G. E. Hunt, S. A. Collins, and R. F. Beebe (1979), Jovian cloud structure and velocity fields, *Nature*, *280*, 776–778.

Morales-Juberias, R., A. Sanchez-Lavega, J. Lecacheux, and F. Colas (2002), A comparative study of Jovian anticyclone properties from a six-year (1994–2000) survey, *Icarus*, *157*, 76–90.

Pedlosky, J. (2008), *Geophysical Fluid Dynamics*, 2nd ed., Academic, Springer, New York.

Perez-Hoyos, S., and A. Sanchez-Lavega (2006a), On the vertical wind shear of Saturn's equatorial jet at cloud level, *Icarus*, *180*, 161–175.

Perez-Hoyos, S., and A. Sanchez-Lavega (2006b), Solar flux in Saturn's atmosphere: Penetration and heating rates in the aerosol and cloud layers, *Icarus*, *180*, 368–378.
Porco, C. C., et al. (2004), Cassini Imaging Science: Instrument characteristics and anticipated scientific investigations at Saturn, *Space Sci. Rev.*, *115*, 363–497.
Read, P. L., T. E. Dowling, and G. Schubert (2009), Saturn's rotation period from its atmospheric planetary-wave configuration, *Nature*, *460*, 608–610.
Sanchez-Lavega, A., J. Lecacheux, F. Colas, and P. Laques (1993), Ground-based observations of Saturn's North Polar spot and hexagon, *Science*, *260*, 329–332.
Sanchez-Lavega, A., J. F. Rojas, J. R. Acarreta, J. Lecacheux, F. Colas, and P. V. Sada (1997), New observations and studies of Saturn's long-lived North Polar spot, *Icarus*, *128*, 322–334.
Sanchez-Lavega, A., et al. (2011), Deep winds beneath Saturn's upper clouds from a seasonal long-lived planetary-scale storm, *Nature*, *475*, 71–74.
Sanchez-Lavega, A., et al. (2012), Ground-based observations of the long-term evolution and death of Saturn's Great White Spot, *Icarus*, *220*, 561–576.
Sayanagi, K. M., U. A. Dyudina, S. P. Ewald, G. Fischer, A. P. Ingersoll, W. S. Kurth, G. D. Muro, C. C. Porco, and R. A. West (2013), Dynamics of Saturn's great storm of 2010–2011 from Cassini ISS and RPWS, *Icarus*, *223*, 460–478.
Showman, A. P. (2007), Numerical simulations of forced shallow-water turbulence: Effects of moist convection on the large-scale circulation of Jupiter and Saturn, *J. Atmos. Sci.*, *64*, 3132–3157.
Smith, B. A., et al. (1979), The Jupiter system through the eyes of Voyager 1, *Science*, *204*, 951–972.
Smith, B. A., et al. (1982), A new look at the Saturn system: The Voyager 2 images, *Science*, *215*, 504–537.
Trammell, H. J., L. Li, X. Jiang, M. Smith, S. Horst, and A. Vasavada (2014), The global vortex analysis of Jupiter and Saturn based on Cassini Imaging Science Subsystem, *Icarus*, *242*, 122–129, doi:10.1016/j.icarus.2014.07.019.
Vasavada, A. R., and A. P. Showman (2005), Jovian atmospheric dynamics: An update after Galileo and Cassini, *Rep. Prog. Phys.*, *68*, 1935–1996.
Vasavada, A. R., S. M. Hörst, M. R. Kennedy, A. P. Ingersoll, C. C. Porco, A. D. Del Genio, and R. A. West (2006), Cassini imaging of Saturn: Southern Hemisphere winds and vortices, *J. Geophys. Res.*, *111*, E05004, doi:10.1029/2005JE002563.
West, R. A. (1983), Spatially resolved methane band photometry of Saturn: II. Cloud structure models at four latitudes, *Icarus*, *53*, 301–309.
Williams, G. P., and T. Yamagata (1984), Geostrophic regimes, intermediate solitary vortices and Jovian eddies, *J. Atmos. Sci.*, *41*, 453–478.